Transactions on Machine Intelligence 4(1) (2021) 36–53

ISSN Online: 2821-1693

Transactions on Machine Intelligence

Journal Homepage: https://tmachineintelligence.ir/index.php/TMI

Noise Reduction in Medical X-Ray Images Using Wavelet and Neural Networks

M. Zamani[1], S. Azadi*[,2], O. Rahmani Seryasat[3]

[1,2] Department of Electrical Engineering, Semnan University, Semnan, Iran
[3]Assistant professor, Department of Electrical Engineering, Shams higher education institute, Gorgan, Iran

ARTICLE INFO

Article History:
Received 5 January 2021
Received in revised form
24 February 2021
Accepted 25 March 2021
Available online 26 March 2021

Keywords:
X-ray Imaging, Wavelet Thresholding, Genetic Algorithm, Directional Adaptive Median Filter (DAMF), Multilayer Neural Networks.

ABSTRACT

Noise reduction in X-ray imaging has been a critical area of research due to its direct impact on image clarity and diagnostic accuracy. This noise primarily results from the reduction of X-ray power, which is necessary to minimize radiation exposure and associated health risks. Traditional noise reduction methods, such as wavelet domain thresholding techniques like BayesShrink, have been widely explored. However, their effectiveness is often limited due to the Poisson-distributed nature of X-ray noise, making standard thresholding approaches suboptimal. In this study, we propose an advanced denoising framework that integrates wavelet domain processing with a genetic algorithm to optimize the BayesShrink threshold. To further enhance image quality, we employ a multi-layer perceptron (MLP) neural network, which improves clarity by refining local pixel intensities. Despite its effectiveness, neural network-based denoising alone struggles to eliminate high-intensity noise. To address this limitation, we introduce a directional adaptive median filter to suppress severe noise while preserving crucial image structures. Since median filtering may compromise edge details, we incorporate an edge reconstruction step to restore essential structural information. Simulation results demonstrate that our proposed approach outperforms conventional methods in terms of Peak Signal-to-Noise Ratio (PSNR), Mean Structural Similarity Index (MSR), and Contrast-to-Noise Ratio (CNR). The findings indicate that our hybrid method provides significantly improved image clarity compared to existing denoising techniques, making it a promising solution for enhancing X-ray image quality while maintaining diagnostic integrity.

1. INTRODUCTION

Noise in medical X-ray images primarily falls into two categories: quantum mottle and artificial noise. Quantum mottle arises due to the statistical nature of X-ray photon detection, while artificial noise results from structural interferences in imaging networks. A key challenge in medical imaging is that reducing X-ray dose, which is

* Corresponding Author: Email: sazadi@semnan.ac.ir
Department of Electrical Engineering, Semnan University

http://dx.doi.org/10.47176/TMI.2021.36

necessary to minimize radiation exposure, increases quantum noise, thereby degrading image quality. Conversely, increasing the X-ray dose improves image clarity but poses significant health risks to patients. Given that X-ray image noise follows a Poisson distribution, it is inherently dependent on the underlying image intensity patterns.

Traditional noise reduction techniques often employ linear adaptive filters, such as the Wiener filter, which utilizes second-order statistics and the Karhunen–Loève (KL) transform to decorrelate image data. In the transformed domain, signal and noise components can be more easily distinguished, allowing for effective noise suppression with minimal signal distortion. Despite its computational efficiency, the Wiener filter often suffers from over-smoothing and induction artifacts, limiting its effectiveness in practical applications.

Nonlinear filtering techniques, such as median filtering, have demonstrated better noise suppression capabilities. By applying a nonlinear smoothing operation over a moving window, median filters effectively remove noise while preserving edges to some extent. However, this approach can still degrade fine structural details, which are critical in medical imaging for detecting fractures, lesions, and other abnormalities.

Recent advancements in wavelet-based denoising have shown promising results in addressing these challenges. Danho [5] and Kamal Abadi et al. [6] proposed wavelet-domain methods for noise reduction, leveraging the two-dimensional wavelet transform (2-D DWT) to decorrelate image data before applying thresholding techniques. One widely used method, BayesShrink (BS), introduced by Chang et al. [7], adaptively adjusts the threshold for each subband to minimize noise while preserving essential image features. However, since Poisson-distributed noise is prevalent in X-ray images, BayesShrink's effectiveness diminishes for high-noise cases, making it more suitable for images with lower noise levels.

To address this limitation, Wang et al. [8] proposed an improved BayesShrink approach that enhances visual quality while preserving edge details. Building on this, our study further refines this method using a hybrid framework that integrates genetic algorithms (GA) and artificial neural networks (ANNs). In recent years, neural networks have been extensively applied in engineering and medical imaging, particularly for nonlinear function estimation [9]. Several studies have explored the integration of wavelet transform with neural networks for noise removal [10-13]. Hong [10] introduced wavelet neural networks, replacing conventional activation functions with wavelet basis functions and incorporating scale and translation parameters for optimized training. Similarly, Lee et al. [14] applied neural networks for X-ray image denoising, but their approach struggled with Poisson noise characteristics, resulting in suboptimal Peak Signal-to-Noise Ratio (PSNR) performance.

Alternative neural network-based denoising techniques include the Transfer Neural Network (TNN), proposed by Zhan [15], in which network weights remain fixed while the activation function dynamically adjusts through a learning mechanism. Adaptive Neuro-Fuzzy Inference Systems (ANFIS) have also been explored for noise reduction, demonstrating promising results [16,17]. However, ANFIS-based methods tend to reduce image resolution as the number of input images increases. In [18], an ANFIS model was employed to estimate threshold values in the wavelet domain, achieving improved PSNR values through optimized threshold selection.

Evolutionary optimization techniques, such as genetic algorithms, have been successfully applied in noise reduction and function approximation tasks [19]. Genetic programming has been utilized to derive adaptive thresholding functions that operate independently of predefined threshold values [19]. In our approach, we employ a genetic algorithm to optimize the threshold estimation process.

This paper presents a novel denoising framework that combines wavelet-based thresholding, genetic algorithms, and neural networks to enhance medical X-ray image quality. Section 1 reviews conventional wavelet thresholding techniques, highlighting their advantages and limitations. Section 2 discusses existing denoising methods, identifying their shortcomings and motivating the need for an improved approach. We introduce a new wavelet-domain thresholding method designed to overcome the limitations of BayesShrink. Our approach first optimizes the BayesShrink threshold using a genetic algorithm, followed by neural network-based training to refine threshold levels for small noise suppression. To address large-amplitude noise, we incorporate a Directional Adaptive Median Filter (DAMF), which effectively preserves edge structures while reducing high-intensity noise.

To evaluate our method, we conducted experiments on real X-ray image datasets and compared its performance against conventional denoising techniques. The results demonstrate that our approach outperforms existing methods

in terms of PSNR, Mean Structural Similarity Index (MSR), and Contrast-to-Noise Ratio (CNR), leading to significantly enhanced image clarity. The final section of this paper presents conclusions and potential directions for future research.

In the subsequent sections, we discuss wavelet-domain noise removal as a key component of our proposed algorithm [7,8,20,22].

2. REMOVING NOISE IN THE WAVELET DOMAIN

In X-ray image acquisition systems, photon noise due to the quantum nature occurs. At low levels of noise follows the Poisson law, the probability distribution is formulated as follows [14]:

$$P(X|\mu) = \frac{\mu^X e^{-\mu}}{X!} \tag{1}$$

This probability function is poison in which the photon x is given with the mean value μ and at the time of ΔT. The standard deviation of this distribution is equal to the square root of the mean. This means that photon noise is dependent on the signal. Two methods commonly used for thresholding, hard thresholding and soft thresholding that are expressed by equations 2 and 3 [20].

$$\delta_\lambda^H(\hat{d}_{jk}) = \begin{cases} 0 & if|\hat{d}_{jk}| \le \lambda \\ \hat{d}_{jk} & if|\hat{d}_{jk}| > \lambda \end{cases} \tag{2}$$

$$\delta_\lambda^S(\hat{d}_{jk}) = \begin{cases} 0 & if\ |\hat{d}_{jk}| \le \lambda \\ \widehat{d}_{jk} - \lambda & if\ \widehat{d}_{jk} > \lambda \\ \widehat{d}_{jk} + \lambda & if\ \hat{d}_{jk} < -\lambda \end{cases} \tag{3}$$

Where λ represents the threshold and d_{jk} denotes the wavelet coefficients of the noisy image. The soft thresholding method is generally preferred over hard thresholding due to its superior denoising performance and ability to preserve image structures more effectively [21].

Although the concept of thresholding is both simple and efficient, selecting an appropriate threshold value remains a challenging task. The universal thresholding method [22] provides an optimal estimate by minimizing the maximum error across all signals. This threshold is determined using the following equation:

$$\lambda = \sigma\sqrt{2logL} \tag{4}$$

Another significant method to obtain an appropriate value for the threshold, is BayesShrink method (BS) [7], which is calculated according to the following equation:

$$T_B = \frac{\sigma^2}{\sigma_X^2} \tag{5}$$

Because we do not have noise characteristics, we apply a Robust Estimator to determine noise standard deviation [23].

$$\sigma = \frac{Median|Y_{ij}|}{0.6747},\ Y_{ij} \in subband \tag{6}$$

Y_{ij} is the wavelet coefficients at the first level of decomposition in the direction of diagonal. To calculate the image noise variance, we have:

$$\sigma_Y^2 = \frac{1}{n^2}\sum_{i,j=1}^{n} X_{ij}^2 \tag{7}$$

Where N^2 is the size of the subband under consideration and X_{ij} is the coefficient of subband under consideration. Also σ_X is estimated as follows:

$$\sigma_X = \begin{cases} \sqrt{\sigma_Y^2 - \sigma^2}, & for\ \sigma_Y^2 > \sigma^2 \\ 0, & for\ \sigma_Y^2 \leq \sigma^2 \end{cases} \tag{8}$$

In the case of $\sigma_Y^2 \leq \sigma^2$, σ_X is zero, in which case T_B is equal to infinite or equal to $T_B = max\ (|X_{i,j}|)$, and hence all the coefficients become zero. Due to increasing levels of the wavelet decomposition of an image, the variance of coefficients increases, correspondingly. Therefore, to reduce the influence of noises in the decomposition level, the BayesShrink thresholding methods was raised. We have [8]:

$$T_B = \alpha \frac{\sigma^2}{\sigma_X^2} \tag{9}$$

Where α varies according to the level subband decomposition and its size:

$$\alpha = \sqrt{\frac{log(n^2)}{2 \times j}} \tag{10}$$

In the following section, we introduce our method for the image noise reduction.

3. THE PROPOSED METHOD

The variance of a Poisson random variable is equal to the average pixel intensity, meaning that the noise level is directly proportional to pixel intensity. This dependency of the signal-to-noise ratio complicates the effectiveness of traditional noise removal methods. Moreover, the noise level varies across different pixel locations within the image.

The peak signal-to-noise ratio (PSNR) follows a linear relationship. Due to the characteristics of Poisson noise, the noise power between wavelet coefficients determined by the wavelet function applied to each pixel varies across the image. Consequently, an effective filtering approach in the wavelet domain must account for these variations. However, the BayesShrink method does not consider these differences, limiting its effectiveness.

Figure 1 provides an overview of the proposed methodology. In the subsequent sections, we introduce the Improved BayesShrink (IBS) thresholding algorithm, along with edge detection and the Directional Adaptive Median Filter (DAMF) in the wavelet domain, designed to enhance noise suppression while preserving image details.

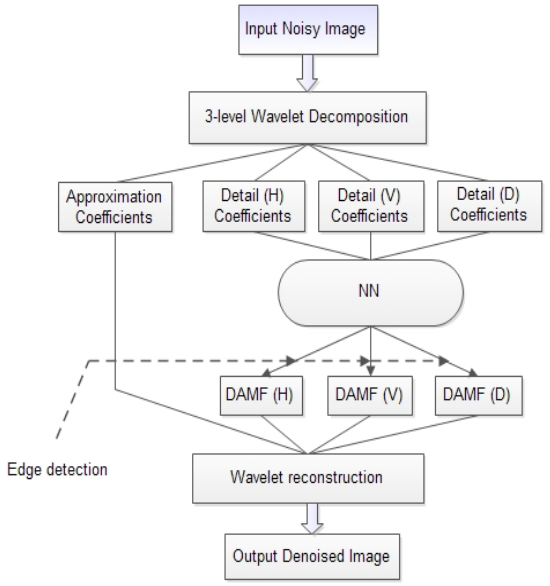

Fig. 1. Schematic of the proposed method.

3.1. Wavelet scheme

In the wavelet transform, images are decomposed into three levels, with each level containing detail subband coefficients in horizontal (H), vertical (V), and diagonal (D) orientations. As a result, the wavelet decomposition produces a total of nine subbands. Increasing the number of decomposition levels enhances the frequency resolution but also increases computational complexity. Therefore, an optimal balance must be maintained to ensure that the frequency characteristics of the image are adequately captured without excessive computational cost.

In this study, we analyze the performance of two wavelet families: Daubechies (Db) and Symlets (Sym). The experimental results demonstrate that the Db wavelet function outperforms the Sym wavelet function in terms of noise reduction and image clarity. Specifically, we utilize the least asymmetric, compactly supported wavelet with four vanishing moments and three scales of orthogonal decomposition.

Table 1 presents the results of the wavelet function's performance on PSNR (Peak Signal-to-Noise Ratio) and computational efficiency. As observed, the db4 wavelet achieves the highest PSNR among the tested wavelet functions. Furthermore, three key statistical parameters average, difference, and difference-to-mean ratio—are notably higher for db4, indicating its superior ability to preserve and extract image details.

Table 1. The effect of wavelet function selection on PSNR and time process.

wavelet		PSNR	mean	max-min	$\frac{\max - \min}{\text{average}}$	Cpu_time
db4	3	**39/89**	**9/19**	**86/83**	**9/29**	4/64
	2	38/16	8/58	72/88	8/49	4/48
db10	3	39/29	9/15	77/19	8/35	4/75
	2	38/1	8/54	67/72	7/93	4/62
sym5	3	39/11	9/11	81/39	8/77	**4/57**
	2	38/17	8/59	65/54	7/62	4/54

3.2. Algorithm BS-GA

Since the wavelet coefficients of X-ray images are generally smaller than those of standard images, the threshold determined by the BayesShrink (BS) method is not optimal for X-ray image denoising. As a result, the BS method fails to effectively suppress noise in X-ray images. To address this limitation, we employ a genetic algorithm (GA) to iteratively optimize the threshold selection process based on the Mean Squared Error (MSE) criterion. This approach ensures that the denoising performance is specifically tailored for X-ray images.

To determine an optimal threshold for each subband, parameter optimization techniques are applied. The methodology follows the workflow illustrated in Figure 2. The initial population in the genetic algorithm consists of multiple chromosomes, where each chromosome represents a set of optimized parameters corresponding to the BS thresholding values for individual wavelet subbands. The fitness function (Equation 1) evaluates the quality of each chromosome by computing the MSE between the original and denoised images. The objective is to minimize this error, thereby improving noise suppression while preserving image details.

$$MSE = \frac{1}{H \times L}\left(\sum_{x=1}^{H}\sum_{y=1}^{L}\left(d(x,y) - o(x,y)\right)\right)^2 \tag{11}$$

Where $d(x,y)$ is denoised image and $\mathrm{o(x,y)}$ is the original image pixels.

Then in the next step, the algorithm uses the fitness value, crossover rate, and mutation rate defined in Table 2 to calculating the next population. Then percentage breakdown of the new population is evaluated recursively. The iteration number of parameter generation is this algorithm is 20. At the end of algorithm, the series achieved the highest fitness was determined. Figure 3 depicts the improvement of thresholding error over the various iterations of the algorithm.

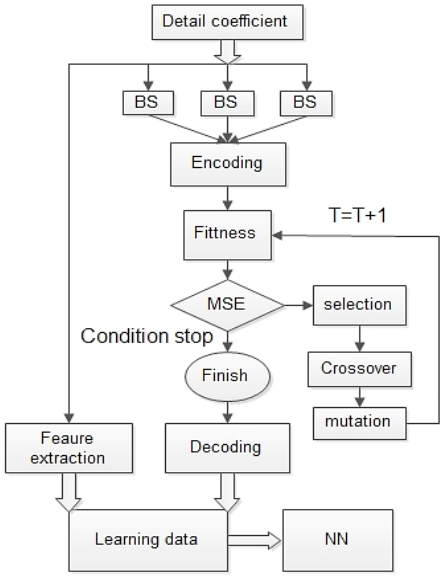

Fig. 2. Optimization BS thresholding method using genetic algorithm.

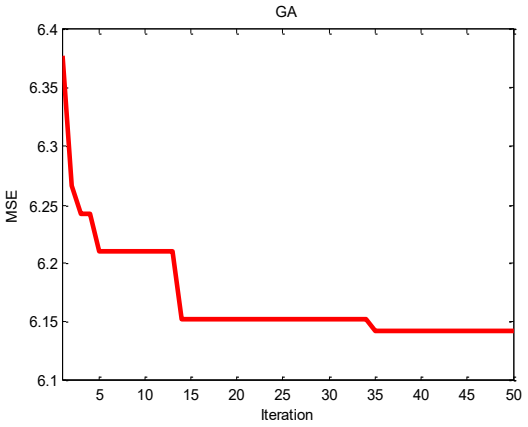

Fig. 3. Progress for Improvement of thresholding error using genetic algorithm.

Table 2. Values of the parameters in genetic algorithm.

Value	Parameter
20	Population
0/3	Keep percent
0/2	Mutation percent
0/5	Cross over percent

3.3. Neural network

In this phase of our research, we implemented a supervised learning approach for training the neural network using additional X-ray images. The subsequent sections provide a detailed explanation of the neural network architecture utilized in this study.

Theoretically, a multilayer perceptron (MLP) neural network with a single hidden layer is sufficient to approximate any continuous function. However, in practical applications, employing two hidden layers often yields superior performance by enhancing the network's ability to capture complex patterns and relationships within the data. Another critical consideration is the selection of an appropriate neural network model for X-ray image denoising. Figure 4 illustrates an overview of the proposed neural network structure, which has been designed to optimize noise reduction while preserving essential image details.

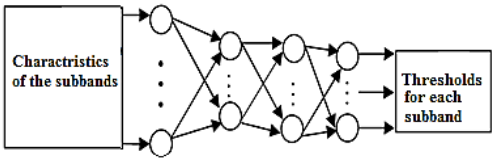

Fig. 4. The structure of neural network used for threshold estimation.

3.3.1. Neural network input data

In our approach, we utilized the methods described in [17, 18] to collect the dataset. For training the neural network, we employed five different X-ray images, each subjected to ten distinct noise levels, resulting in a total of 50 images for training. To optimize the threshold selection for each wavelet subband, we applied genetic algorithms (GA). This process enabled us to determine the most effective threshold values for denoising. Figure 2 presents the flowchart outlining the neural network training process.

Our proposed method can be summarized as follows:

1. Adding Poisson noise to the image according to the following formula [8]:

$$g(n, m) = \frac{1}{\lambda} \times poisson\{\lambda \times f(n, m)\} \quad (12)$$

Where $f(n, m)$ is original image and $poisson\{f\}$ is a Poisson noise generator. Also, λ sets the intensity of the Poisson noise in the X-ray image. The value of lambda increases with increasing the noise intensity.

2. Calculate the wavelet transform of all versions of the noise created in step 1 in three levels.

3. Calculate the optimum value of the mean, variance, and smoothness all versions noise. These values are input of the neural network input.

4.Determine the optimum threshold level of wavelet coefficients of the noisy image in Step 2. The target of NN is the threshold level obtained from GA.

Thus, for each image, we would have 9 subband that each one dedicated to one subband. This threshold level is the output data to train the neural network.

3.3.2. Training neural network

In this study, we implemented a feedforward neural network (FNN) with two hidden layers, containing six and nine neurons, respectively. After testing various learning algorithms, we determined that the backpropagation learning method was the most effective. Other methods resulted in higher errors, whereas backpropagation demonstrated greater stability and resilience in the presence of noise.

For training the neural network, we employed the Gradient Descent with Momentum (GDM) and Adaptive Learning Rate. Backpropagation was used to compute the performance derivative concerning bias and weight variables. Each variable was adjusted using steepest descent with instantaneous momentum updates.

The specific parameters for training were:

- Momentum coefficient: 0.8
- Learning rate: 0.1
- Number of iterations (Epochs): 30,000

These parameters were chosen to enhance convergence speed and minimize errors in threshold optimization for X-ray image denoising.

3.3.3. Testing the neural network

After training the neural network, we evaluated its performance using two distinct sets of test images. Noise was artificially introduced into these images, and we computed key statistical characteristics of each wavelet subband, including mean, variance, and smoothness. These extracted features served as inputs to the neural network. The trained neural network then estimated the optimal threshold values for each subband.

In the subsequent step, a soft thresholding function was applied based on the predicted threshold levels to effectively suppress noise in the wavelet domain. This function selectively attenuated wavelet coefficients, minimizing noise while preserving essential image details. Notably, the test data used in this phase were generated under conditions similar to the training phase, ensuring consistency in network performance.

This process was repeated five times for each training image and noise level. The results were then compared with existing denoising methods, as summarized in Tables 3 and 4.

Performance Evaluation:

- Figure 6 presents the error progression during neural network learning, showcasing network performance across three phases: training, validation, and testing.

- Figure 7 depicts the regression analysis of the neural network. The high correlation coefficient (0.8) suggests that the network effectively learned the mapping between input features and optimal threshold values, ensuring robust noise reduction.

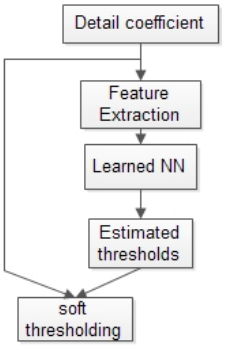

Fig. 5. Threshold estimation using neural network during the test.

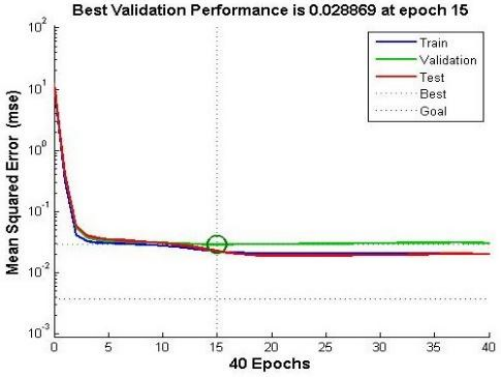

Fig. 6. The error-learning neural network and its performance in the training, validation and testing.

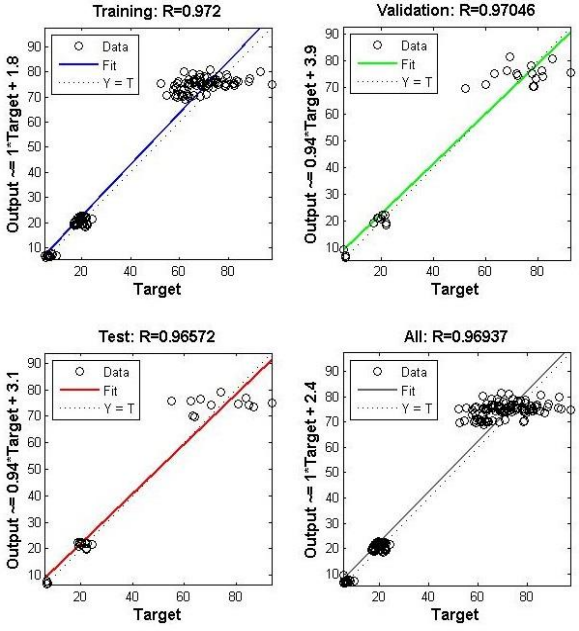

Fig. 7. Regression plot. As can be seen; by selecting the appropriate features, the network is able to fit the data with a high correlation coefficient.

3.3.4. Edge detection in wavelet domain

If DAMF filter be applied to threshold wavelet coefficients with thresholding IBS method, the edges are removed along with the noise. This filter is not able to distinguish the difference between edge and big amplitudes of the noise. Since edge information is important for detecting detail of the picture, therefore, we used a modified edge detection algorithm on the wavelet coefficients.

In order to detect edges in image, with the fact that whenever the absolute values of wavelet coefficients are big, are considered as the edge, the edge detection algorithm operates.

The steps of the algorithm are as follows [8]:

1. Sorting the values of the threshold coefficients of wavelet from high to low for each subband:

$$W = \{w_1, \cdots, w_i, \cdots, w_N\} \tag{13 A}$$

2. Calculating the sum of the sorted coefficients, SUM_n and SUM_N as follows:

$$SUM_n = \sum_{i=1}^{n} abs(w_i)^2 \tag{13 B}$$

$$SUM_N = \sum_{i=1}^{N} abs(w_i)^2 \tag{13 C}$$

3. Selecting the thresholding value in each subband according to the following equation:

$$r = \frac{SUM_n}{SUM_N} \tag{14}$$

When $r > v$, that v is the keep percent of a particular edge and in this paper have been chosen equal to 0.8, w_n choose as the threshold of the edge detector.

4. Detecting the edges of the coefficients in each subband according to the following algorithm:

If $abs\ (w_i)^2 > \ abs\ (w_n)^2$, w_i is selected as an edge, otherwise w_i is noise and must be removed by the DAMF filter. After detecting edges, the large amplitudes of noise are eliminated using DAMF

3.3.5. Directional adaptive median filter (DAMF)

Small amplitude noise is effectively mitigated using the BayesShrink (BS) method, but the large amplitude Poisson noise proves more challenging to suppress. To address this, we applied the Directional Adaptive Median Filter (DAMF) on the thresholded wavelet coefficients obtained after the BS-GA (Genetic Algorithm) optimization process. The DAMF is effective in reducing large amplitude noise while preserving essential image details.

The median filter [9] is a nonlinear filtering technique commonly used to eliminate shot noise from images. Its advantage lies in its ability to preserve edges without significantly distorting them. However, it does tend to lose smaller details, such as sharp corners or fine textures.

In Figure 8, the DAMF window is depicted for three directions: horizontal, vertical, and diagonal, which correspond to the detail subbands of the wavelet transform. Additionally, the DAMF window applied to the diagonal at angles 45° and 135° is shown in the figure. The selection of the window is based on calculating the difference between pixel values, as this metric helps identify large amplitude noise, which is typically characterized by larger coefficient values.

To compute the difference, the absolute values of wavelet coefficients are arranged in ascending order. For the directions 45° and 135°, the difference between adjacent coefficients is calculated to identify areas with significant variations in intensity, which are typically indicative of large amplitude noise. This approach ensures that the filtering process focuses on regions with high noise while preserving the underlying image structure.

$$d1 = \left||A(i-1,j-1)| - |A(i+1,j+1)|\right| \quad \text{(15 A)}$$

$$d2 = \left||A(i-1,j+1)| - |A(i+1,j-1)|\right| \quad \text{(15 B)}$$

Where $A(i,j)$ is selected wavelet coefficients. If $d_1 \geq d_2$, we choose the wavelet coefficients for direction of 145° and otherwise we choose 45° to process. Figure 8 shows these computations.

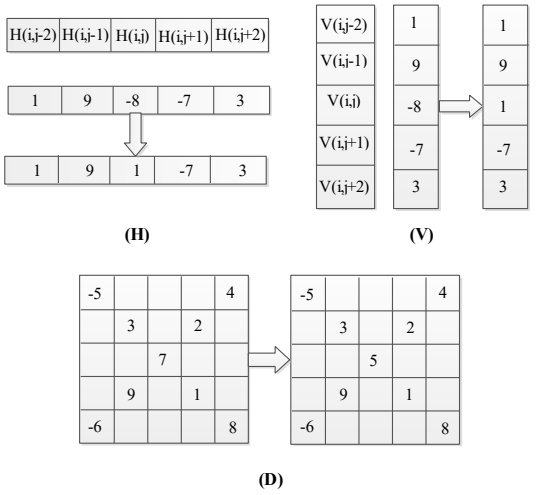

$135°: [1\ 3\ 5\ 7\ 8] \quad d1 = |3-7| = 4 \quad d1 > d2$
$45°: [2\ 4\ 6\ 7\ 9] \quad d1 = |4-7| = 3$

Fig. 8. Structure of directional adaptive median filter DAMF [8].

4. DISCUSSION AND RESULTS

In this section, we evaluate the performance of the proposed method by applying it to different X-ray images. Due to the absence of reference X-ray images for calculating the Peak Signal-to-Noise Ratio (PSNR), we used an image with a high dose as the reference image.

The results of applying various mother wavelet functions, the number of vanishing moments, and the number of decomposition levels are summarized in Table 1. The findings indicate that selecting the Daubechies wavelet function with 4 vanishing moments and 3 decomposition levels yields the highest PSNR, demonstrating optimal performance in noise reduction.

To further validate our proposed method, we compared it against other denoising techniques such as Median Filtering (MF), Wiener Filtering (WF), and the BayesShrink (BS) method. The PSNR was used to quantify the level of distortion between the reference image and the denoised image. Additionally, we utilized Mean Structural Similarity Ratio (MSR) and Contrast-to-Noise Ratio (CNR) parameters to assess the quality of the denoised images. The following sections describe how these parameters were calculated:

4.1. Types of evaluation criteria

4.1.1. The signal-noise ratio (PSNR):

$$PSNR = 10 \times log_{10}\left(\frac{Pixel_{max}^2}{MSE}\right) \quad (16)$$

Where MSE is the mean squared error (Equation 1) and $Pixel_{max}$ is peak intensity of the pixel in the image.

4.2. Image quality evaluation criteria [24-25]

4.2.1. Mean to standard deviation ratio (MSR)

$$MSR = \frac{\mu_d}{\sigma_d} \tag{17}$$

4.2.2. Contrast to noise ratio (CNR)

$$CNR = \frac{|\mu_d - \mu_u|}{\sqrt{0.5(\sigma_d^2 + \sigma_u^2)}} \tag{18}$$

Where M_d and σ_d are the mean, and standard deviation in the desired area (DROI) as a window onto the image edges. Furthermore, μ_u and σ_u are the mean and standard deviation in the undesired area (UROI) as a window in the background. The results obtained for each of these methods are shown in Tables 3 and 4. Figures 9A to 9C, show the superiority of the proposed approach with other methods.

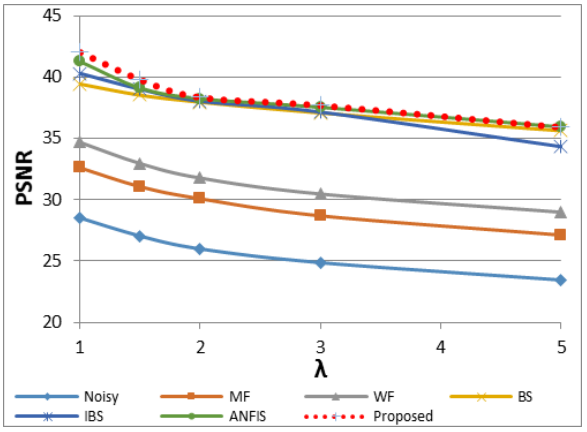

Fig. 9A. PSNR comparison of the proposed method and the previous methods for several different levels of noise.

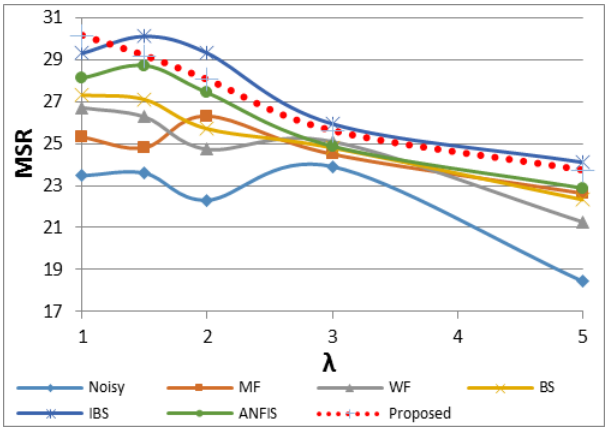

Fig. 9B. MSR comparison of the proposed method and the previous methods for several different levels of noise.

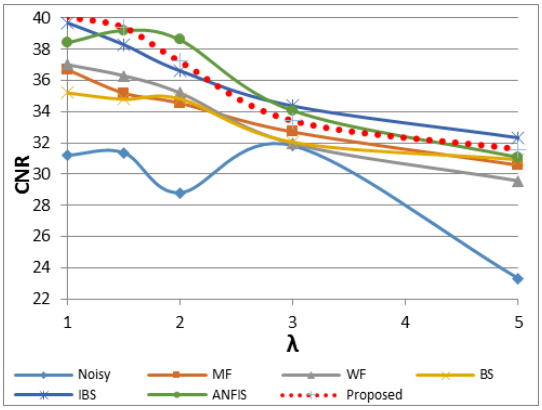

Fig. 9C. CNR comparison of the proposed method and the previous methods for several different levels of noise**.**

Table 3. Assessing Results of different methods for knee photo.

Method		Noisy	MF	WF	BS	IBS	ANFIS	proposed
$\lambda = 1$	PSNR	28/52	32/61	34/69	39/44	40/3	41/28	**42/03**
	MSR	23/47	25/31	26/71	27/31	29/3	28/12	**30/14**
	CNR	31/21	36/71	37/02	35/21	39/7	38/41	**40/07**
$\lambda = 1/5$	PSNR	27/04	31/07	32/96	38/53	39	39/12	39/8
	MSR	23/59	24/81	26/27	27/1	30/1	28/72	29/18
	CNR	31/38	35/2	36/31	34/8	38/3	39/2	**39/41**
$\lambda = 2$	PSNR	25/99	30/08	31/77	37/96	38	38/24	**38/37**
	MSR	22/31	26/31	24/73	25/71	29/3	27/43	**28/04**
	CNR	28/81	34/55	35/21	34/83	36/6	38/61	**37/22**
$\lambda = 3$	PSNR	24/87	28/69	30/47	37/08	37/2	37/54	**37/71**
	MSR	23/91	24/5	25/1	24/8	25/9	24/88	25/61
	CNR	31/83	32/71	31/96	32/05	34/4	34/07	33/4
$\lambda = 5$	PSNR	23/45	27/11	28/98	35/62	34/3	35/94	**35/94**
	MSR	18/44	22/63	21/27	22/33	24/1	22/88	23/73
	CNR	23/31	30/57	29/57	30/93	32/3	31/07	31/57

Table 4. Assessing Results of different methods for head and neck photos.

Method		Noisy	MF	WF	BS	IBS	ANFIS	proposed
$\lambda = 1$	PSNR	29/11	32/86	35/66	37/64	37/8	38/41	**39/21**
	MSR	13/69	13/89	14	14/16	14/5	15/01	14/47
	CNR	38/9	40/99	40/65	41	41/8	41/17	**42/42**
$\lambda = 1/5$	PSNR	27/67	31/44	33/73	36/76	38	41/02	**40/46**
	MSR	12/21	13/65	13/13	13/67	13/9	14/09	14/18
	CNR	34/81	35/31	34/98	35/88	37/1	37/32	36/82
$\lambda = 2$	PSNR	26/74	30/7	32/97	36/47	37/2	37/18	**38/41**
	MSR	11/81	13/88	13/5	13/58	13/9	13/87	14/09
	CNR	32/15	33/12	35/04	34/15	36/2	34/93	35/98
$\lambda = 3$	PSNR	25/33	29/35	30/85	35/85	36/3	36/91	**37/74**
	MSR	10/94	13/55	12/57	13/12	13/9	13/54	13/81
	CNR	26/66	31/62	28/88	30/88	33/1	31/88	32/65
$\lambda = 5$	PSNR	23/84	27/53	29/1	34/95	35/2	35/56	34/98
	MSR	8/64	11/58	11/01	11/9	13/1	12/5	12/6
	CNR	23/02	26/99	28/41	25/93	28/7	27/62	27/67

Denoised image are shown in Figures 12 and 13. These Figures indicating the results of the denoising methods of median filter, Wiener filter, BS method [7], IBS method [8], ANFIS [17] and the proposed method. WF is an optimal filter that is able to achieve the desired amount of mean square error. Since this method is based on linear filters, may be in areas of image, noise reinforce and thus arises Patches in the image. Also, MF effectively reduced the shot noise in the picture but one of the disadvantages is that many of detail along to picture be lost. Because as mentioned earlier this filter cannot distinguish the difference between details of image, and high values of noises.

According to the results shown in Figure 10-c, picture is blurred and many fine details of the picture disappeared. In BS method, the noises effectively reduced having the borders maintained.

IBS method also further reduce noise, and preserve edges more effectively, has provided a clearer picture compared with BS. ANFIS method using the algorithm presented in [17] has been implemented, and has been able to achieve a high rate of improvement in noise reduction, but the image quality and the edges is reduced. Our proposed approach results in reduced image noise as shown in Figure 10-h. The proposed method is able to effectively reduce the noise compared to other methods, the visual quality of the image to protect and preserve the fine details of the image.

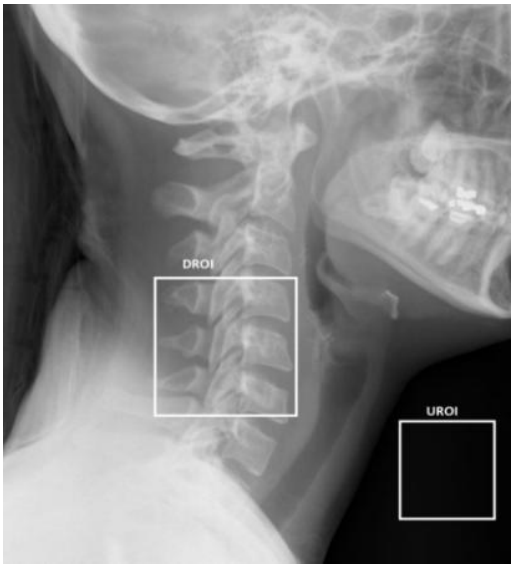

Fig.10. Original image of the head and neck.

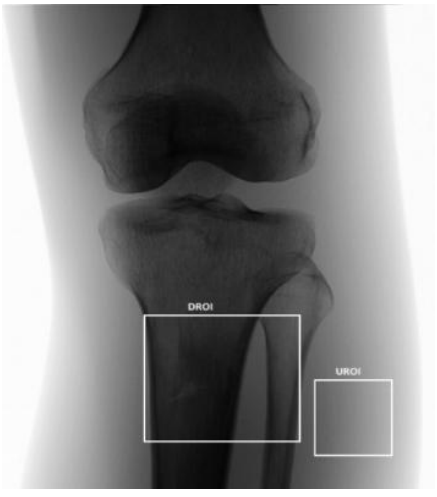

Fig. 11. Original image of the knee.

(a) Original

(b) Noisy, PSNR=28.52 MSR=23.47 CNR=31.21

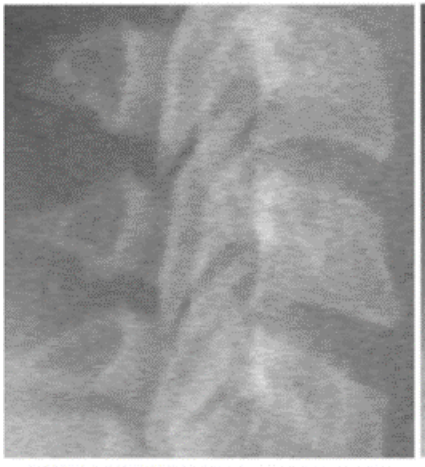

(c) MF, PSNR=32.61 MSR=25.31 CNR=36.71

(d) WF, PSNR=34.69 MSR=26.71 CNR=37.02

(e) BS, PSNR=39.44 MSR=27.31 CNR=35.21

(f) IBS, PSNR=40.31 MSR=29.3 CNR=39.71

Fig. 12. Original and noisy image ($\lambda = 1$) and the results of each method.

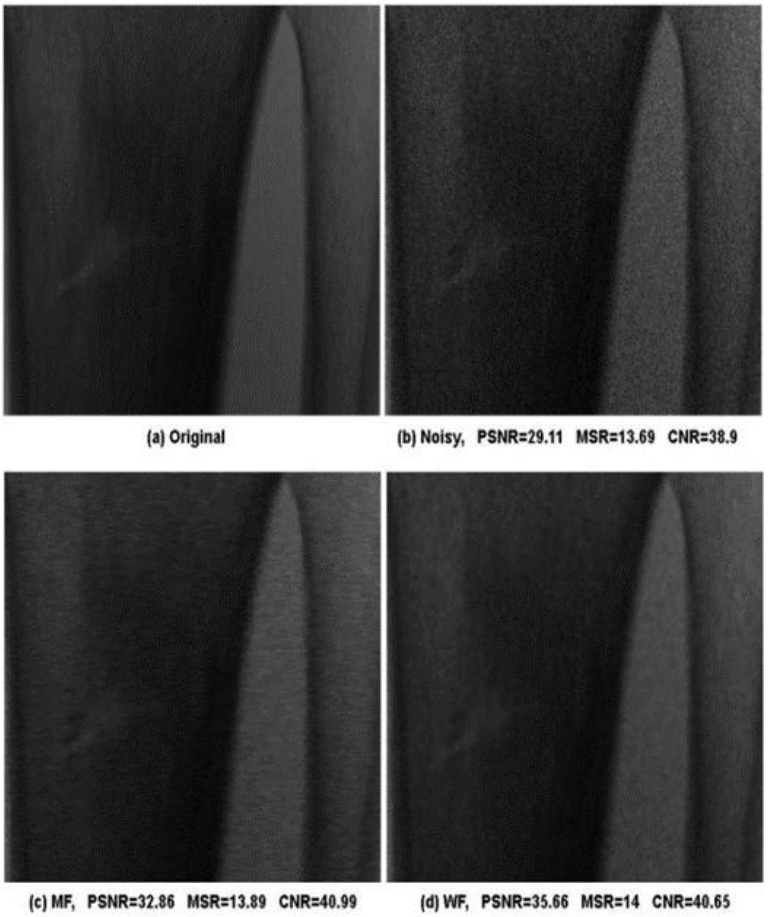

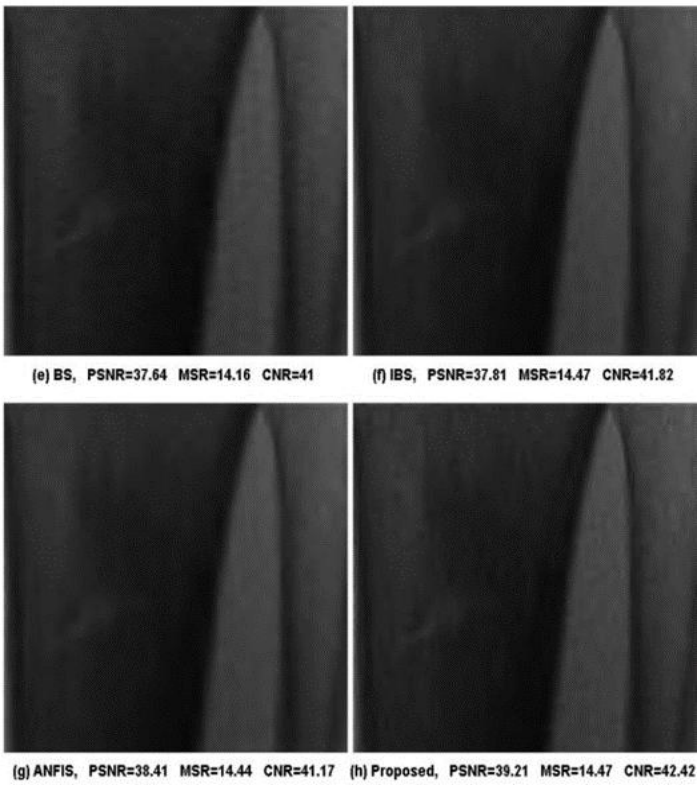

Fig. 13. Original and noisy image ($\lambda = 1$) and the results of each method.

5. CONCLUSION

This paper studies the problem of noise reduction in medical X-ray images. In this way, we need to design a number of assumptions and limitations of handling the proposed methods. In order to improve reducing the noise, we proposed a new method in the wavelet domain. Firstly, processed the wavelet coefficient using BS-GA method, and then trained the neural network according to these criteria. Then, we could achieve the optimal threshold for other images and different noise intensities. This method obtained results and better PSNR value in different images. Our future studies would be on finding the threshold for other types of medical images. All the wavelet functions with different types of noise can be further work in this field.

CONFLICTS OF INTEREST

The authors declare no conflict of interest.

REFERENCES

[1] Okamoto, T., Furui, S., Ichiji, H., Yoshino, S., Lu, J., & Yahagi, T. (2004). Noise reduction in digital radiography using wavelet packet based on noise characteristics. Journal of Signal Processing, 8(6), 485-494. https://doi.org/10.2299/jsp.8.485

[2] Nowak, R. D., & Baraniuk, R. G. (1999). Wavelet-domain filtering for photon imaging systems. IEEE Transactions on Image Processing: A Publication of the IEEE Signal Processing Society, 8(5), 666-678. https://doi.org/10.1109/83.760334

[3] Ozkan, M. K., Erdem, A. T., Sezan, M. I., & Tekalp, A. M. (1992). Efficient multiframe Wiener restoration of blurred and noisy image sequences. IEEE Transactions on Image Processing: A Publication of the IEEE Signal Processing Society, 1(4), 453-476. https://doi.org/10.1109/83.199916

[4] Wang, Z., & Zhang, D. (1999). Progressive switching median filter for the removal of impulse noise from

highly corrupted images. IEEE Transactions on Circuits and Systems II Analog and Digital Signal Processing, 46(1), 78-80. https://doi.org/10.1109/82.749102

[5] Donoho, D. L., Johnstone, I. M., Kerkyacharian, G., & Picard, D. (1995). Wavelet shrinkage: Asymptopia? Journal of the Royal Statistical Society, 57(2), 301-337. https://doi.org/10.1111/j.2517-6161.1995.tb02032.x

[6] Atkinson, I., Kamalabadi, F., Mohan, S., & Jones, D. L. (2004). Wavelet-based 2-D multichannel signal estimation. In Proceedings 2003 International Conference on Image Processing (Cat. No. 03CH37429) (pp. 33-38). IEEE. https://doi.org/10.1109/icip.2003.1246636

[7] Chang, S. G., Yu, B., & Vetterli, M. (2000). Adaptive wavelet thresholding for image denoising and compression. IEEE Transactions on Image Processing: A Publication of the IEEE Signal Processing Society, 9(9), 1532-1546. https://doi.org/10.1109/83.862633

[8] Wang, L., Lu, J., Li, Y., Yahagi, T., & Okamoto, T. (2005). Noise reduction using wavelet with application to medical X-ray image. In 2005 IEEE International Conference on Industrial Technology (pp. 33-38). IEEE. https://doi.org/10.1109/ICIT.2005.1600606

[9] Kavchak, M. A., & Budman, H. M. (1998). Adaptive neural network architectures for nonlinear function estimation. In Proceedings of the 1998 American Control Conference. ACC (IEEE Cat. No. 98CH36207). Philadelphia, PA, USA. https://doi.org/10.1109/ACC.1998.694629

[10] Yin, Z., Shi, W., Wu, Z., & Zhang, J. (2022). Multilevel wavelet-based hierarchical networks for image compressed sensing. Pattern Recognition, 129, 108758. https://doi.org/10.1016/j.patcog.2022.108758

[11] Chen, X.-L., Tian, M., & Yao, W.-B. (2005). GPR signals de-noising by using wavelet networks. In 2005 International Conference on Machine Learning and Cybernetics (pp. 869-873). IEEE. https://doi.org/10.1109/icmlc.2005.1527766

[12] Lotrič, U. (2004). Wavelet based denoising integrated into multilayered perceptron. Neurocomputing, 62, 179-196. https://doi.org/10.1016/j.neucom.2004.02.003

[13] Zhang, X.-P. (2002). Space-scale adaptive noise reduction in images based on thresholding neural network. In 2001 IEEE International Conference on Acoustics, Speech, and Signal Processing (Vol. 4, pp. 2185-2188). IEEE. https://doi.org/10.1109/ICASSP.2001.941313

[14] Li, Y., Lu, J., Wang, L., & Takashi, Y. (2009). Denoising by using multineural networks for medical X-ray imaging applications. Neurocomputing, 72(13-15), 2884-2891. https://doi.org/10.1016/j.neucom.2008.07.019

[15] Mastriani, M., & Giraldez, A. E. (2018). Microarrays denoising via smoothing of coefficients in wavelet domain. arXiv. http://arxiv.org/abs/1807.11571

[16] Liu, P., & Li, H. (2002). Image restoration techniques based on fuzzy neural networks. Science in China Series F: Information Sciences, 45(4), 273-285. https://doi.org/10.1360/02yf9024

[17] Norouzzadeh, Y., & Katebi, S. D. (2006). Application of ANFIS in Wavelet Denoising. In 6th Iranian Conference on Fuzzy Systems and 1st Islamic World Conference on Fuzzy Systems (Islamic Azad University of Shiraz).

[18] Norouzzadeh, Y., & Rashidi, M. (2011). Image denoising in wavelet domain using a new thresholding function. In International Conference on Information Science and Technology (pp. 62-66). Nanjing, China. https://doi.org/10.1109/ICIST.2011.5765347

[19] Norouzzadeh, Y., & Katebi, S. D. (2007). Threshold estimation in wavelet domain using fuzzy rules. In 4th Iranian Conference on Machine Vision and Image Processing.

[20] Antoniadis, A., Bigot, J., & Sapatinas, T. (2001). Wavelet estimators in nonparametric regression: A comparative simulation study. Journal of Statistical Software, 6(6). https://doi.org/10.18637/jss.v006.i06

[21] Donoho, D. L. (1995). De-noising by soft-thresholding. IEEE Transactions on Information Theory, 41(3), 613-627. https://doi.org/10.1109/18.382009

[22] Donoho, D. L., & Johnstone, I. M. (1994). Ideal spatial adaptation by wavelet shrinkage. Biometrika, 81(3), 425-455. https://doi.org/10.1093/biomet/81.3.425

[23] Donoho, D. L., & Johnstone, I. M. (1995). Adapting to unknown smoothness via wavelet shrinkage. Journal of the American Statistical Association, 90(432), 1200-1224. https://doi.org/10.1080/01621459.1995.10476626

[24] Soltanian-Zadeh, H., Windham, J. P., & Yagle, A. E. (1995). A multidimensional nonlinear edge-preserving filter for magnetic resonance image restoration. IEEE Transactions on Image Processing: A Publication of the IEEE Signal Processing Society, 4(2), 147-161. https://doi.org/10.1109/83.342189

[25] Cincotti, G., Loi, G., & Pappalardo, M. (2001). Frequency decomposition and compounding of ultrasound medical images with wavelet packets. IEEE Transactions on Medical Imaging, 20(8), 764-771. https://doi.org/10.1109/42.938244